

IGNIS: A Robust Neural Network Framework for Constrained Parameter Estimation in Archimedean Copulas

Agnideep Aich^{1*}

¹ Department of Mathematics, University of Louisiana at Lafayette,
Lafayette, Louisiana, USA.

Abstract

Classical estimators, the cornerstones of statistical inference, face insurmountable challenges when applied to important emerging classes of Archimedean copulas. These models exhibit pathological properties, including numerically unstable densities, non-monotonic parameter-to-dependence mappings, and vanishingly small likelihood gradients, rendering methods like Maximum Likelihood (MLE) and Method of Moments (MoM) inconsistent or computationally infeasible. We introduce **IGNIS**, a unified neural estimation framework that sidesteps these barriers by learning a direct, robust mapping from data-driven dependency measures to the underlying copula parameter θ . IGNIS utilizes a multi-input architecture and a theory-guided output layer ($\text{softplus}(z) + 1$) to automatically enforce the domain constraint $\hat{\theta} \geq 1$. Trained and validated on four families (Gumbel, Joe, and the numerically challenging A1/A2), IGNIS delivers accurate and stable estimates for real-world financial and health datasets, demonstrating its necessity for reliable inference in modern, complex dependence models where traditional methods fail.

IGNIS Network, Archimedean Copulas, Parameter Estimation, Neural Networks, Dependency Modeling

MSC 2020 Subject Classification: 62H05, 62H12, 62F10, 68T07, 62-08

1. Introduction

Maximum Likelihood Estimation (MLE), a pillar of statistical inference, is the gold standard for parameter estimation due to its desirable asymptotic properties. Its efficacy, however, is predicated on well-behaved likelihood functions. In the domain of dependence modeling using copulas [Nelsen, 2006], this assumption can dramatically fail. For a growing class of flexible and important models, such as the novel A1 and A2 Archimedean copulas [Aich et al., 2025], the likelihood function exhibits pathological properties that render classical estimation methods inconsistent, unstable, or computationally infeasible. This issue is not isolated; numerical challenges in copula estimation are a known and significant concern in high-stakes applications like quantitative risk management [Hofert et al., 2013].

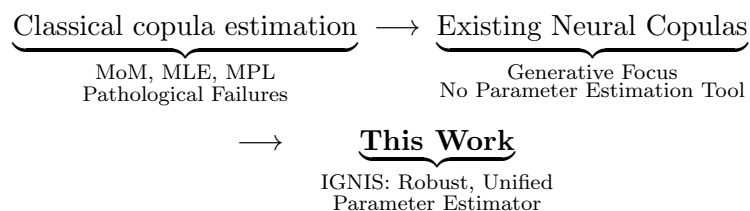
Our analysis of these challenging models reveals three fundamental barriers that make classical estimation untenable:

1. **Numerical Instability from Boundary Singularities:** The copula density function, which is required for MLE, explodes near the boundaries of the unit hypercube due to ill-behaved generator derivatives (e.g., with singularities of order $O(t^{-3})$), leading to floating-point overflow during computation.

*Corresponding author: Agnideep Aich, agnideep.aich1@louisiana.edu, ORCID: [0000-0003-4432-1140](https://orcid.org/0000-0003-4432-1140)

2. **Non-Monotonic Dependence Mappings:** The relationship between the canonical dependence measure, Kendall’s τ , and the copula parameter θ can be non-monotonic. This makes the Method of Moments (MoM) ill-posed, as a single empirical τ value can map to multiple, distinct θ values.
3. **Vanishing Gradients and Hessian Decay:** For even moderately large values of θ , the log-likelihood surface becomes pathologically flat. The score function decays polynomially to zero (e.g., $O(\theta^{-8})$), causing gradient-based optimizers to stall prematurely. Second-order information decays even faster, rendering Newton-like methods useless.

Recent deep learning approaches have shown immense promise in statistics, but have not addressed this specific estimation problem. The state-of-the-art has largely focused on generative tasks, such as learning new copula generators from scratch [Ling et al., 2020, Ng et al., 2021] or modeling highly complex, high-dimensional dependence structures [Ng et al., 2022]. However, the fundamental problem of robust parameter estimation for known, specified families that exhibit the aforementioned pathologies remains a critical open gap. To fill this gap, we introduce **IGNIS**, a unified neural estimation framework that sidesteps the pitfalls of classical methods entirely.



IGNIS learns a direct mapping from a vector of robust, data-driven summary statistics to the underlying copula parameter θ . Our main contributions are:

1. The identification and formal analysis of three critical optimization barriers that cause classical estimators to fail for an important class of copula models.
2. The design and implementation of IGNIS, a unified neural architecture that learns a robust estimation function and enforces theoretical parameter constraints ($\hat{\theta} \geq 1$) via a custom output layer.
3. A comprehensive validation on simulated and real-world data, demonstrating that IGNIS provides accurate and stable estimates precisely in the regimes where traditional methods break down.

The remainder of this paper is organized as follows. Section 2 reviews related work. Section 3 presents necessary preliminaries. Section 4 provides motivation for our work. Section 5 details the IGNIS architecture and training protocol. Section 6 presents the simulation results for IGNIS, and Section 7 demonstrates real-data applications. Finally, Section 8 concludes and outlines future research directions.

2. Related Work

Our work builds upon two distinct streams of literature: classical parameter estimation for copulas and the emerging field of deep learning for statistical modeling.

2.1 Classical Estimation and its Limitations

Parameter estimation for Archimedean copulas has traditionally been approached via two main routes. The Method of Moments (MoM), particularly using Kendall’s τ or Spearman’s ρ , is valued for its computational simplicity and circumvention of the likelihood function [Genest and Rivest, 1993]. However, its validity hinges on a strictly monotonic relationship between the dependence measure and the parameter θ , a condition that, as we show, does not hold for the A1 copula family.

The second route is Maximum Likelihood Estimation (MLE) or its semi-parametric variant, Maximum Pseudo-Likelihood (MPL) [Genest et al., 1995]. While asymptotically efficient, MLE requires computing the copula density, which can be analytically complex and numerically unstable. Efforts by [Hofert et al., 2011] derived explicit generator derivatives to make MLE more feasible for standard families. Yet, subsequent large-scale studies confirmed that even with these advances, classical estimators face significant numerical challenges and potential unreliability, especially in high dimensions or for complex models [Hofert et al., 2013]. The A1 and A2 families are prime examples where these numerical pathologies become insurmountable barriers, necessitating a new approach.

2.2 Deep Learning Approaches to Copula Modeling

The recent intersection of deep learning and copula modeling has been dominated by powerful generative approaches that learn or approximate the generator function itself, rather than estimating parameters of a pre-defined family. For instance, ACNet [Ling et al., 2020] introduced a neural architecture to learn completely monotone generator functions, enabling the approximation of existing copulas and the creation of new ones. Similarly, [Ng et al., 2021] proposed a generative technique using latent variables and Laplace transforms to represent Archimedean generators, scaling to high dimensions. Other work has focused on non-parametric inference for more flexible classes like Archimax copulas, which are designed to model both bulk and tail dependencies [Ng et al., 2022].

While these methods represent the state-of-the-art in constructing flexible, high-dimensional dependence models, they do not address the targeted problem of estimating the parameter θ for a specified family, especially when that family exhibits the estimation pathologies we have identified. Broader work on Physics-Informed Neural Networks (PINNs) has shown the power of deep learning for solving problems with known physical constraints [Raissi et al., 2019, Sirignano and Spiliopoulos, 2018], but a specialized framework for constrained parameter estimation in statistically challenging copula models has been a missing piece. IGNIS is designed specifically to fill this gap, providing a discriminative estimator that is robust, constraint-aware, and applicable across multiple families where classical methods fail.

3. Preliminaries

3.1 Copulas and Dependency Modeling

Copulas are statistical tools that model dependency structures between random variables, independent of their marginal distributions. Introduced by Sklar [1959], they provide a unified approach to capturing joint dependencies. Archimedean copulas, known for their simplicity and flexibility, are defined using a generator function, making them particularly effective for modeling bivariate and multivariate dependencies.

3.2 The A1 and A2 Copulas

Like all Archimedean copulas, the novel A1 and A2 copulas [Aich et al., 2025] are defined through generator functions $\phi(t)$ that are continuous, strictly decreasing, and convex on $[0, 1]$, with $\phi(1) = 0$. The A1 and A2 copulas extend the Archimedean copula framework to capture both upper and lower tail dependencies more effectively. In general, an Archimedean copula is given by:

$$C(u, v) = \phi^{-1}(\phi(u) + \phi(v)). \quad (1)$$

For the A1 copula, the generator and its inverse are defined as:

$$\phi_{A1}(t; \theta) = \left(t^{1/\theta} + t^{-1/\theta} - 2\right)^\theta, \quad \theta \geq 1, \quad (2)$$

$$\phi_{A1}^{-1}(t; \theta) = \left[\frac{t^{1/\theta} + 2 - \sqrt{(t^{1/\theta} + 2)^2 - 4}}{2} \right]^\theta, \quad \theta \geq 1. \quad (3)$$

Similarly, for the A2 copula:

$$\phi_{A2}(t; \theta) = \left(\frac{1-t}{t}\right)^\theta (1-t)^\theta, \quad \theta \geq 1, \quad (4)$$

$$\phi_{A2}^{-1}(t; \theta) = \frac{t^{1/\theta} + 2 - \sqrt{(t^{1/\theta} + 2)^2 - 4}}{2}, \quad \theta \geq 1. \quad (5)$$

The exact formula of the Kendall's τ for A1 and A2 copulas are given by (See Appendix A for full derivations)

$$\tau_{A1} = 1 + 2[\psi(\theta) - \psi(\theta + \frac{1}{2})], \quad (6)$$

$$\tau_{A2} = 1 - \frac{6 - 8 \ln 2}{\theta}. \quad (7)$$

Both copulas are parameterized by $\theta \geq 1$, which governs the strength and nature of the dependency. The dual tail-dependence structure of A1 and A2 copulas is particularly valuable for modeling extreme co-movements in joint distributions. In financial risk management, they can capture simultaneous extreme losses (lower-tail) and windfall gains (upper-tail), improving estimates of portfolio tail risk. In anomaly detection, they identify coordinated extreme events (e.g., simultaneous sensor failures in industrial systems or cyber attacks across networks) by quantifying asymmetric tail dependencies. This flexibility makes them superior to single-tailed copulas e.g., Clayton (captures only lower tails) and Gumbel (captures only upper tail) in scenarios where both tail behaviors are critical.

3.3 Simulation from Archimedean Copulas

In this section, we present an algorithm introduced by Genest and Rivest [1993] to generate an observation (u, v) from an Archimedean copula C with generator ϕ .

The above algorithm is a consequence of the fact that if U and V are uniform random variables with an Archimedean copula C , then $W = C(U, V)$ and $S = \frac{\phi(U)}{\phi(U) + \phi(V)}$ are independent, S is uniform $(0, 1)$, and the distribution function of W is K . In our implementation, the inverse function $K^{-1}(y)$ is computed numerically using a robust root-finding algorithm (specifically, the bisection method).

Algorithm 1 Bivariate Archimedean Copula Sampling (Genest et al., 1993)

Require: Generator ϕ , its derivative ϕ' , inverse ϕ^{-1}

Ensure: A single draw (u, v) from the copula

- 1: Draw $s, t \stackrel{\text{iid}}{\sim} \text{Uniform}(0, 1)$
- 2: Define

$$K(x) = x - \frac{\phi(x)}{\phi'(x)}, \quad K^{-1}(y) = \sup\{x \mid K(x) \leq y\}$$

- 3: Compute $w \leftarrow K^{-1}(t)$
- 4: Compute

$$u \leftarrow \phi^{-1}(s\phi(w)), \quad v \leftarrow \phi^{-1}((1-s)\phi(w))$$

- 5: **return** (u, v)
-

3.4 Method of Moments Estimation

The Method of Moments (MoM) is a classical statistical technique for parameter estimation, where theoretical moments of a distribution are equated with their empirical counterparts. In the context of copula modeling, MoM is particularly advantageous when direct likelihood-based estimation is challenging due to the complexity of deriving tractable probability density functions.

In this work, we derive exact analytical formulas for Kendall's τ for both A1 and A2 copulas (see Appendix A). These formulas establish a direct relationship between Kendall's τ and the copula parameter θ , allowing for robust parameter estimation. By inverting this relationship, we develop MoM estimators for θ , providing a practical approach for modeling dependencies in scenarios where traditional methods like MLE and MPL may be ineffective. However, in Section 4.2, we see that for especially A1 and even for A2, MoM is not the most efficient estimator.

4. Motivation

4.1 Limitations in Parameter Estimation Using Method of Moments

In this section, we present the results of a simulation study to estimate the parameter θ for the A1 and A2 copulas using the **Method of Moments (MoM)**. The simulation is conducted using the **algorithm** as described in Section 3.3.

4.2 Results for MoM

Simulation Setup

- 1.: The simulation is performed for $\theta = \{2.0, 5.0, 10.0\}$.
- 2.: $n = 100,000$ pairs (u, v) are generated for each scenario.
- 3.: The parameter θ is estimated using the **Method of Moments (MoM)**, where the sample Kendall's τ is matched with the theoretical $\tau(\theta)$.
- 4.: Standard errors (SE) for the estimates of θ are computed using the method described in Genest et al. [2011].

Table 1 summarizes MoM estimation results for A1 and A2:

Table 1: Method-of-Moments Estimates and Standard Errors for A1 and A2

True θ	Copula	Est. θ	SE(θ)
2.0	A1	4.4860	0.1597
2.0	A2	1.9047	0.0709
5.0	A1	9.5215	0.8844
5.0	A2	4.9398	0.2335
10.0	A1	6.1183	1.2273
10.0	A2	9.4366	0.1900

For A1, MoM estimates are inconsistent (e.g., the estimate for true $\theta = 10.0$ is lower than that for 5.0). For A2, MoM performs quite well compared to A1. The problem in A1 occurs due to the non-monotonicity between A1 and its Kendall's τ which implies that MoM cannot uniquely recover θ ; the estimator seems to be inconsistent. MoM will also fail when the sample Kendall's τ falls outside the theoretical range of the copula model, rendering parameter estimation infeasible in such scenarios. This is highly likely for A2 copula because of its high Kendall's τ lower bound of 0.545 which is relatively higher than sample Kendall's τ of many real-world datasets.

It is to be noted that the one-parameter copula families researchers use in practice are generally ordered by positive quadrant dependence (PQD), so that the dependence parameter is in one-to-one correspondence with standard nonparametric measures of dependence such as Kendall's tau or Spearman's rho. Unfortunately, such is not the case for model A1. Indeed, it is possible to find two values of theta which correspond to the same value of Kendall's tau. This is an important limitation for A1.

It is also to be noted that the injectivity property of the copula generator function guarantees that each distinct value of the parameter θ produces a unique copula, ensuring the mathematical validity of the model which is true for A1 (See Appendix B). This is not the same as the relationship between A1's θ and its Kendall's τ which is not one-to-one so that identical values of τ may correspond to different θ values. This fundamental difference motivates the use of a neural network approach, which leverages multiple summary features to accurately estimate θ despite the ambiguity in the θ - τ relationship.

4.3 Limitations in Parameter Estimation Using Maximum Likelihood and Maximum Pseudo-Likelihood

While the Method of Moments faces fundamental limitations with A1/A2 copulas, classical likelihood-based approaches, Maximum Likelihood Estimation (MLE) and Maximum Pseudo-Likelihood (MPL), prove equally problematic due to pathological properties of the generator functions. The non-standard forms of ϕ_{A1} and ϕ_{A2} induce three critical optimization barriers (See Appendix D for full derivations).

4.3.1 Three Critical Optimization Barriers

1. Numerical Instability in Density Calculations As $t \rightarrow 0^+$ (with θ fixed), the second derivatives of the generators blow up:

$$|\phi''_{A1}(t)| \sim O(t^{-3}), \quad |\phi''_{A2}(t)| \sim O(t^{-\theta-2}).$$

(See Figures 1a & 1b.) Hence the copula density

$$c(u, v) = \frac{\partial^2}{\partial u \partial v} C(u, v)$$

overflows once

$$\text{A1: } t < \varepsilon_{\text{mach}}^{1/3}, \quad \text{A2: } t < \varepsilon_{\text{mach}}^{1/(\theta+2)},$$

with $\varepsilon_{\text{mach}} \approx 2.22 \times 10^{-16}$.

2. Vanishing Gradients (Score-Decay) As $\theta \rightarrow \infty$ (with $t \in (0, 1)$ fixed), the log-likelihood score decays:

$$|\partial_\theta \ell(\theta)| = \begin{cases} O(n \theta^{-8}), & \text{A1,} \\ O(n \theta^{-3}), & \text{A2.} \end{cases}$$

Thus it falls below any fixed tolerance $\varepsilon_{\text{grad}}$ once

$$n \theta^{-k} < \varepsilon_{\text{grad}},$$

which for $\varepsilon_{\text{grad}} = 10^{-6}$ and $n = 1000$ yields

$$\theta_{\text{crit}}^{\text{A1}} \approx 8.2, \quad \theta_{\text{crit}}^{\text{A2}} \approx 126.$$

(See Figures 1c & 1d.)

3. Hessian Decay (Barrier 3) Again as $\theta \rightarrow \infty$ (with t fixed), the scalar Hessian decays even faster:

$$|\partial_\theta^2 \ell(\theta)| = \begin{cases} O(n \theta^{-9}), & \text{A1,} \\ O(n \theta^{-4}), & \text{A2.} \end{cases}$$

In double precision ($\varepsilon_{\text{mach}} \approx 2.22 \times 10^{-16}$) this underflows once

$$n \theta^{-9} < \varepsilon_{\text{mach}} \implies \theta > \left(\frac{n}{\varepsilon_{\text{mach}}} \right)^{1/9} \approx 1.2 \times 10^2,$$

$$n \theta^{-4} < \varepsilon_{\text{mach}} \implies \theta > \left(\frac{n}{\varepsilon_{\text{mach}}} \right)^{1/4} \approx 4.6 \times 10^4.$$

(See Figures 1e & 1f.)

Figure 1 helps with the visualization of the three barriers.

Hybrid approaches, using MoM to initialize MLE/MPL, remain infeasible as well since for **A1**, the non-monotonic τ - θ mapping yields multiple θ candidates and for **A2**, the theoretical bound $\tau > 0.545$ often excludes common datasets because of its relative high lower τ bound value compared to other copulas. These structural limitations necessitate bypassing both moment inversion and likelihood optimization, motivating our neural framework IGNIS.

5. Methodology: IGNIS Network

Named after the Latin word for “fire,” the IGNIS Network is a unified neural estimator for four Archimedean copula families (Gumbel, Joe, A1, A2), each with the same parameter domain $\theta \geq 1$.

Reproducibility: All experiments use a fixed seed (123) applied globally across Python’s `random` module, NumPy, TensorFlow, and PyTorch to ensure full computational reproducibility. Code runs on Python 3.11 with TensorFlow 2.19, SciPy 1.15.3, and scikit-learn 1.6.1.

Input Representation: Each example is a 9-D vector $x = [f; c]$, where

1. $f \in \mathbf{R}^5$ consists of five dependency measures: empirical Kendall’s τ , Spearman’s ρ , upper tail-dependence at the 0.95 quantile (λ_{upper}), lower tail-dependence at the 0.05 quantile (λ_{lower}), and the Pearson correlation coefficient (r).
2. $c \in \{0, 1\}^4$ is a one-hot encoded vector identifying the copula family.

Network Architecture: Let $x \in \mathbf{R}^8$. We apply:

$$h_1 = \text{ReLU}(W_1 x + b_1), \quad (128)$$

$$h_2 = \text{ReLU}(W_2 h_1 + b_2), \quad (128)$$

$$h_3 = \text{ReLU}(W_3 h_2 + b_3), \quad (64)$$

$$\theta_{\text{raw}} = W_4 h_3 + b_4 \in \mathbf{R}.$$

A `softplus` activation plus 1 enforces $\hat{\theta} \geq 1$:

$$\hat{\theta} = \text{softplus}(\theta_{\text{raw}}) + 1.$$

Figure 2 illustrates this flow.

Training Data Generation: For each family, we sample 500 θ values uniformly from the range $[1, 20]$. For each θ , we simulate $n = 5,000$ pairs (U, V) using Algorithm 1 (Section 3.3), compute the five summary features for the vector f , and concatenate the corresponding one-hot vector c . This process yields a total of $500 \times 4 = 2000$ training examples.

Feature Scaling: We standardize all 9-D inputs using scikit-learn’s `StandardScaler`. The scaler is fitted only on the training data split and then applied to transform both the validation and test sets.

Hyperparameters: In Table 2 we see that training uses MSE loss with Adam [Kingma and Ba, 2014] (5×10^{-4}), batch size 32, max 200 epochs, early stopping (patience 20 on 20% validation).

Table 2: Key Hyperparameters

Hyperparameter	Value
Batch size	32
Learning rate	5×10^{-4}
Optimizer	Adam
Max epochs	200
Early-stop patience	20
Train/val split	80/20
Bootstrap replicates	100

Uncertainty Quantification: For each test (U, V) sample, we draw $B = 100$ bootstrap replicates, recompute $\{f\}$, re-predict $\hat{\theta}$, and report $\text{SE}(\hat{\theta}) = \text{std}(\{\hat{\theta}^{(b)}\})$.

Implementation Details: IGNIS is implemented in TensorFlow/Keras with He-uniform initialization for all Dense layers. All training was performed on an NVIDIA GeForce RTX 4060 Laptop GPU, where each epoch (50 steps at ≈ 4 ms/step, batch size 32) takes about 2 s.

Theoretical Soundness: One-hot encoding ensures family identifiability. Under regularity conditions (Appendix C), $\hat{\theta} \xrightarrow{p} \theta$. The softplus+1 transform guarantees $\hat{\theta} \in [1, \infty)$.

Figure 2 illustrates the IGNIS architecture. An 9-D input vector (four dependency measures + one-hot copula ID) is processed by three fully-connected layers (128–128–64 ReLU, He-uniform), and a final softplus+1 activation guarantees $\hat{\theta} \geq 1$.

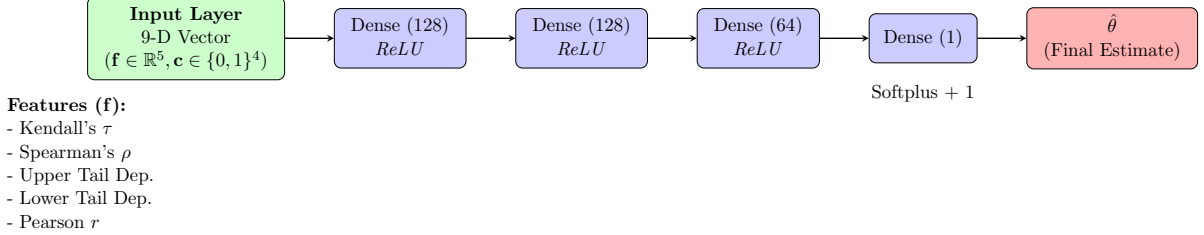


Figure 2: The updated IGNIS Architecture. A 9-D input vector (five dependency measures, \mathbf{f} , and a 4-D one-hot family identifier, \mathbf{c}) is processed by three ReLU-activated hidden layers. A final dense layer followed by a Softplus+1 activation enforces the constraint $\hat{\theta} \geq 1$.

6. Simulation Studies for IGNIS

The same simulation setup described in Section 5 is followed here for $\theta = \{2.0, 5.0, 10.0\}$.

Table 3 show performance of the IGNIS network on simulated data.

Table 3: IGNIS Network Estimation Results for All Copulas

Copula	True θ	Est. θ	Bootstrap SE(θ)
True $\theta = 2.0$			
Gumbel	2.0	2.06	0.08
Joe	2.0	1.88	0.07
A1	2.0	2.05	0.13
A2	2.0	1.96	0.10
True $\theta = 5.0$			
Gumbel	5.0	5.07	0.23
Joe	5.0	4.88	0.12
A1	5.0	4.96	0.13
A2	5.0	4.81	0.18
True $\theta = 10.0$			
Gumbel	10.0	9.92	0.25
Joe	10.0	9.56	0.24
A1	10.0	9.68	0.29
A2	10.0	9.65	0.35

Key observations: For both A1 and A2, the IGNIS network is able to recover the true value of the parameter used to generate the data used in simulation. We see how especially for A1, there is no issue like in the case of MoM. The non-monotonic mapping in the A1 copula that severely undermines MoM estimation does not affect the IGNIS network, since it learns directly from data and do not require such monotonicity. Also, this network works extremely well for Gumbel and Joe copulas.

In our neural network framework, the estimated dependence parameter θ is obtained via a direct mapping from summary dependency measures to θ . To quantify the uncertainty of these estimates, we employ a bootstrap procedure. For each test sample, multiple bootstrap replicates are generated by resampling the (U,V) pairs. The summary features are recomputed for each bootstrap replicate, and the trained network is used to predict θ . The standard deviation of these bootstrap predictions provides a robust estimate of the standard error, thereby reflecting both the sampling variability and the inherent uncertainty in the neural network’s predictions.

7. Real-World Applications

We validate IGNIS using two distinct domains where copulas are widely applied: financial markets (AAPL–MSFT stock returns) and public health (CDC Diabetes Dataset). These applications demonstrate the network’s versatility across data types. For clarity, we emphasize this is an estimation methodology demonstration, not a copula selection analysis.

The IGNIS network estimates θ through the following standardized workflow:

1. Data Preprocessing:

Financial Data: Attain stationarity via log-returns:

$$r_t = \log(P_t/P_{t-1}),$$

where P_t are adjusted closing prices.

Healthcare Data: We use original variables (GenHlth, PhysHlth) without differencing.

For both domains, transform marginals to pseudo-observations via rank-based PIT:

$$u_i = \frac{\text{rank}(x_i)}{n+1}, \quad v_i = \frac{\text{rank}(y_i)}{n+1},$$

yielding $\{(u_i, v_i)\}_{i=1}^n \in [0, 1]^2$ with approximately uniform margins.

2. Feature Extraction:

From the paired pseudo-observations, we compute five dependence measures: (1) Empirical Kendall’s τ , (2) Spearman’s ρ , (3) upper tail-dependence $\lambda_{upper} = \frac{1}{n} \sum_{i=1}^n \mathbf{1}\{u_i > 0.95, v_i > 0.95\}$, (4) lower tail-dependence $\lambda_{lower} = \frac{1}{n} \sum_{i=1}^n \mathbf{1}\{u_i < 0.05, v_i < 0.05\}$, and (5) the Pearson correlation coefficient. These form the feature vector $\mathbf{f} \in \mathbb{R}^5$.

3. Input Construction:

The feature vector \mathbf{f} is concatenated with a one-hot encoded copula identifier $\mathbf{c} \in \{0, 1\}^4$ for the families Gumbel, Joe, A1, and A2. This creates the final 9-dimensional input vector $\mathbf{x} = [\mathbf{f}; \mathbf{c}]$. This vector is then standardized using the STANDARDSCALER that was fitted on the simulated training data.

4. Theta Estimation:

The network architecture consists of three hidden layers with 128, 128, and 64 ReLU-activated units, each initialized using the He initialization scheme. The final layer applies a softplus activation followed by a unit shift to guarantee that $\hat{\theta} \geq 1$. We train the IGNIS network using the Adam optimizer with a learning rate of 5×10^{-4} and a mean-squared error loss function for 200 epochs. During training, 20% of the data are held out for validation, and early stopping with a patience of 20 epochs is employed to prevent overfitting.

5. Uncertainty Quantification:

To quantify uncertainty, we perform a bootstrap procedure by resampling the pseudo-observations with replacement $B = 100$ times. For each bootstrap resample, we recompute the four features

and obtain a corresponding estimate $\hat{\theta}^{(b)}$. The bootstrap standard error of $\hat{\theta}$ is then calculated as the sample standard deviation of these bootstrap estimates:

$$\widehat{\text{SE}}(\hat{\theta}) = \text{std}(\hat{\theta}_{\text{boot}}).$$

Results for both applications are presented in Tables 4 and 5, following identical estimation protocols for cross-domain comparability.

7.1 Dataset 1: AAPL-MSFT Returns Dataset

Source and Period: The dataset [Aroussi, 2024] comprises daily adjusted closing prices for two stocks, AAPL and MSFT, obtained from `yfinance` library in Python. Data were collected for the period from January 1, 2020 to December 31, 2023.

Variables: The primary variable of interest is the adjusted closing price for each ticker. This column (labeled either as `Adj Close` or `Close`) reflects the price after accounting for corporate actions such as dividends and stock splits.

Derived Measures: From the raw price data, daily log returns are computed. These log returns serve as a proxy for the instantaneous rate of return and are stationary.

7.1.1 Estimation Results

Table 4 summarizes the parameter estimation.

Table 4: Estimated θ Values and Bootstrap Standard Errors from Financial Data

Copula	Estimated θ	Bootstrap SE(θ)
Gumbel	2.6771	0.2186
Joe	3.5701	0.3411
A1	1.2324	0.0638
A2	1.1986	0.0770

7.2 Dataset 2: CDC Diabetes Dataset

Source: We programmatically retrieved the CDC Diabetes Health Indicators dataset (UCI ML Repository ID 891) using the `ucimlrepo` Python package [Centers for Disease Control and Prevention, 2023]. The full dataset contains 253,680 respondents and 21 original features; for our analysis we pulled only the two raw columns `GenHlth` and `PhysHlth`.

Variables: From these two columns we constructed empirical pseudo-observations via the probability integral transform (PIT), i.e.

$$u_i = \frac{\text{rank}(\text{GenHlth}_i)}{n + 1}, \quad v_i = \frac{\text{rank}(\text{PhysHlth}_i)}{n + 1},$$

where $n = 253,680$. These appear in our pipeline as:

1. `GenHlth_pu`: u_i , the pseudo-value for general health
2. `PhysHlth_pu`: v_i , the pseudo-value for physical health

7.2.1 Estimation Results

Table 5 summarizes the parameter estimation.

Table 5: Estimated θ Values and Bootstrap Standard Errors from CDC Diabetes Data

Copula	Estimated θ	Bootstrap SE(θ)
Gumbel	1.4570	0.0029
Joe	2.5876	0.0058
A1	1.4220	0.0054
A2	1.2299	0.0023

7.3 Key Observations

The IGNIS Network successfully estimates theta from three different datasets. IGNIS offers a robust, accurate, and computationally efficient alternative to traditional methods. The unified framework of IGNIS simplifies parameter estimation across various copula families making it an universal tool.

8. Conclusion and Future Work

In this paper, we confronted the critical failure of classical estimation methods when applied to an important class of Archimedean copulas with pathological likelihoods. We demonstrated that numerical instabilities, non-monotonic dependence mappings, and vanishing gradients make traditional inference via Maximum Likelihood or the Method of Moments inconsistent and computationally infeasible. To solve this, we introduced the **IGNIS Network**, a deep learning framework that provides robust, constraint-aware parameter estimates by learning a direct mapping from data-driven statistics. By leveraging a multi-layer architecture and a theory-guided **softplus+1** output layer, IGNIS delivers accurate and stable estimates for multiple copula families, succeeding precisely where classical methods fail.

The practical implications of IGNIS extend particularly to extreme-value analysis where A1/A2’s dual tail-dependence structure provides critical advantages. In financial systems, it enables risk analysts to reliably model joint tail events (e.g., market crashes or insurance claims during natural disasters) using A1/A2’s dual-tail flexibility, improving capital allocation and hedging strategies. For anomaly detection in industrial IoT networks, it identifies coordinated failure patterns where sensors exhibit asymmetric tail dependencies. Healthcare applications include modeling comorbid extreme health episodes where patients experience simultaneous deterioration of multiple health indicators. By solving the parameter estimation challenge for these advanced copulas, IGNIS unlocks their potential for **real-time risk assessment** and **multivariate anomaly detection systems**.

Despite these strengths, IGNIS has several limitations. First, our evaluation has been restricted to four bivariate Archimedean families; commonly used generators such as Clayton and Frank remain to be integrated. Second, the current architecture handles only two-dimensional dependencies, so extending to multivariate or nested copulas will require permutation-invariant or graph-based neural designs. Third, reliance on a fixed set of four summary statistics may limit performance in small-sample or heavy-tailed scenarios, suggesting that adaptive or richer feature representations could enhance robustness. Finally, IGNIS assumes a known family identifier via one-hot encoding, leaving fully automated copula selection as an open challenge.

Looking ahead, we see several promising directions for future work. Incorporating Clayton, Frank, and other Archimedean generators will broaden IGNIS’s applicability. High-dimensional extensions can be pursued by designing architectures, such as DeepSets or attention-based graphs, that respect permutation symmetry in multivariate dependence. To capture dynamic relationships, we plan to integrate recurrent or temporal-attention modules that adapt to time-varying copulas. We can use alternative features (e.g., Blomqvist’s β , Gini’s γ) in the future. Joint inference of copula family and parameter via mixture-of-experts or multi-task learning would eliminate the need for a priori family tagging. Also, we plan to conduct a rigorous comparative performance study between the IGNIS framework and global optimization methods, such as Particle Swarm Optimization (PSO) and Genetic Algorithms (GA). On the uncertainty front, embedding Bayesian neural networks or deep ensembles can provide principled credible intervals for $\hat{\theta}$. Finally, exploring alternative summary features, such as higher-order tail-dependence coefficients or distance-based metrics, may further improve estimation under challenging data regimes. Together, these extensions will help establish IGNIS as a comprehensive, data-driven toolkit for dependence modeling across diverse applications.

Statements and Declarations

Funding

The authors did not receive any funding for this research.

Competing Interests

The authors have no relevant financial or non-financial interests to disclose.

Data Availability

The data that support the findings of this study are available from publicly accessible sources and are provided in the manuscript.

References

- A. Aich, A. B. Aich, and B. Wade. Two new generators of archimedean copulas with their properties. *Communications in Statistics - Theory and Methods*, 2025.
- R. Aroussi. yfinance: Yahoo! finance market data downloader, 2024. Python Package Index, version 0.2.28 (<https://github.com/ranaroussi/yfinance>).
- Centers for Disease Control and Prevention. Cdc diabetes health indicators, 2023. (<https://doi.org/10.24432/C53919>).
- C. Genest and L.-P. Rivest. Statistical inference procedures for bivariate archimedean copulas. *Journal of the American Statistical Association*, 88(423):1034–1043, 1993.
- C. Genest, K. Ghoudi, and L.-P. Rivest. A semiparametric estimation procedure of dependence parameters in multivariate families of distributions. *Biometrika*, 82:543–552, 1995.
- C. Genest, J. Nešlehová, and N. Ben Ghorbal. Estimators based on kendall’s tau in multivariate copula models. *Australian & New Zealand Journal of Statistics*, 53(2):157–177, 2011.

- M. Hofert, M. Mächler, and A. J. McNeil. Likelihood inference for archimedean copulas, 2011. arXiv preprint (<https://arxiv.org/pdf/1108.6032>).
- M. Hofert, M. Mächler, and A. J. McNeil. Archimedean copulas in high dimensions: Estimators and numerical challenges motivated by financial applications. *Journal de la Société Française de Statistique*, 154(1):25–79, 2013.
- K. Hornik. Approximation capabilities of multilayer feedforward networks. *Neural Networks*, 4(2):251–257, 1991.
- D. P. Kingma and J. Ba. Adam: A method for stochastic optimization. In *Proceedings of the 3rd International Conference on Learning Representations (ICLR)*, 2014.
- C. K. Ling, F. Fang, and J. Z. Kolter. Deep archimedean copulas. In *Proceedings of the 34th Conference on Neural Information Processing Systems (NeurIPS 2020)*, 2020.
- R. B. Nelsen. *An Introduction to Copulas*. Springer, 2006.
- Y. Ng, A. Hasan, K. Elkhail, and V. Tarokh. Generative archimedean copulas. In *Proceedings of the 37th Conference on Uncertainty in Artificial Intelligence (UAI 2021)*, 2021.
- Y. Ng, A. Hasan, and V. Tarokh. Inference and sampling for archimax copulas. In *Proceedings of the 36th Conference on Neural Information Processing Systems (NeurIPS 2022)*, 2022.
- M. Raissi, P. Perdikaris, and G. E. Karniadakis. Physics-informed neural networks: A deep learning framework for solving forward and inverse problems involving nonlinear partial differential equations. *Journal of Computational Physics*, 378:686–707, 2019.
- J. Sirignano and K. Spiliopoulos. Dgm: A deep learning algorithm for solving partial differential equations. *Journal of Computational Physics*, 375:1339–1364, 2018.
- A. Sklar. Fonctions de répartition à n dimensions et leurs marges. *Publications de l’Institut de Statistique de l’Université de Paris*, 8:229–231, 1959.
- E. E. Slutsky. Über stochastische asymptoten und grenzwerte. *Metron – Rivista Internazionale di Statistica*, 5(1):3–89, 1925.
- A. W. van der Vaart and J. A. Wellner. *Weak Convergence and Empirical Processes: With Applications to Statistics*. Springer, 1996.
- H. White. Some asymptotic results for learning in single hidden-layer feedforward neural network models. *Journal of the American Statistical Association*, 84:1003–1013, 1989.

A. Appendix: Full Derivation of Kendall’s τ for A1 and A2 Copulas

In this appendix, we derive explicit analytical expressions for Kendall’s τ for the novel Archimedean copulas A1 and A2. These derivations form the theoretical basis for the Method-of-Moments estimation of the copula parameter θ .

A.1 Derivation for the A1 Copula

For a general Archimedean copula with generator $\varphi(t)$, Kendall's τ is given by

$$\tau = 1 + 4 \int_0^1 \frac{\varphi(t)}{\varphi'(t)} dt.$$

For the A1 copula the generator is

$$\varphi_{A1}(t; \theta) = \left(t^{1/\theta} + t^{-1/\theta} - 2 \right)^\theta, \quad \theta \geq 1.$$

Step 1: Differentiation of $\varphi_{A1}(t; \theta)$ Differentiate $\varphi_{A1}(t; \theta)$ with respect to t using the chain rule:

$$\varphi'_{A1}(t; \theta) = \theta \left(t^{1/\theta} + t^{-1/\theta} - 2 \right)^{\theta-1} \cdot \frac{d}{dt} \left[t^{1/\theta} + t^{-1/\theta} - 2 \right].$$

Since

$$\frac{d}{dt} t^{1/\theta} = \frac{1}{\theta} t^{1/\theta-1} \quad \text{and} \quad \frac{d}{dt} t^{-1/\theta} = -\frac{1}{\theta} t^{-1/\theta-1},$$

it follows that

$$\varphi'_{A1}(t; \theta) = \theta \left(t^{1/\theta} + t^{-1/\theta} - 2 \right)^{\theta-1} \left[\frac{1}{\theta} t^{1/\theta-1} - \frac{1}{\theta} t^{-1/\theta-1} \right].$$

Cancelling the factor θ we have:

$$\varphi'_{A1}(t; \theta) = \left(t^{1/\theta} + t^{-1/\theta} - 2 \right)^{\theta-1} \left[t^{1/\theta-1} - t^{-1/\theta-1} \right].$$

Step 2: Form the Ratio $\varphi_{A1}/\varphi'_{A1}$ Taking the ratio,

$$\begin{aligned} \frac{\varphi_{A1}(t; \theta)}{\varphi'_{A1}(t; \theta)} &= \frac{\left(t^{1/\theta} + t^{-1/\theta} - 2 \right)^\theta}{\left(t^{1/\theta} + t^{-1/\theta} - 2 \right)^{\theta-1} \left[t^{1/\theta-1} - t^{-1/\theta-1} \right]} \\ &= \frac{t^{1/\theta} + t^{-1/\theta} - 2}{t^{1/\theta-1} - t^{-1/\theta-1}}. \end{aligned}$$

After some algebra (by expressing numerator and denominator in a common form), one can show that this expression simplifies to

$$\frac{\varphi_{A1}(t; \theta)}{\varphi'_{A1}(t; \theta)} = \frac{t \left(t^{1/\theta} - 1 \right)}{1 + t^{1/\theta}}.$$

Step 3: Change of Variables Set

$$u = t^{1/\theta} \implies t = u^\theta, \quad dt = \theta u^{\theta-1} du.$$

Changing variables, the integral becomes

$$\begin{aligned} \int_0^1 \frac{\varphi_{A1}(t; \theta)}{\varphi'_{A1}(t; \theta)} dt &= \int_0^1 \frac{u^\theta (u - 1)}{1 + u} \theta u^{\theta-1} du \\ &= \theta \int_0^1 \frac{u^{2\theta-1} (u - 1)}{1 + u} du. \end{aligned}$$

Step 4: Express the Integral as a Series Denote

$$I(\theta) = \theta \int_0^1 \frac{u^{2\theta-1}(u-1)}{1+u} du.$$

Note that

$$u^{2\theta-1}(u-1) = u^{2\theta} - u^{2\theta-1}.$$

Thus,

$$I(\theta) = \theta \left[\int_0^1 \frac{u^{2\theta}}{1+u} du - \int_0^1 \frac{u^{2\theta-1}}{1+u} du \right].$$

For $u \in [0, 1]$ we can expand

$$\frac{1}{1+u} = \sum_{n=0}^{\infty} (-1)^n u^n.$$

Then,

$$\int_0^1 \frac{u^{2\theta}}{1+u} du = \sum_{n=0}^{\infty} (-1)^n \int_0^1 u^{2\theta+n} du = \sum_{n=0}^{\infty} \frac{(-1)^n}{2\theta+n+1},$$

and similarly,

$$\int_0^1 \frac{u^{2\theta-1}}{1+u} du = \sum_{n=0}^{\infty} \frac{(-1)^n}{2\theta+n}.$$

Thus,

$$I(\theta) = \theta \sum_{n=0}^{\infty} (-1)^n \left[\frac{1}{2\theta+n+1} - \frac{1}{2\theta+n} \right].$$

Since

$$\frac{1}{2\theta+n+1} - \frac{1}{2\theta+n} = -\frac{1}{(2\theta+n)(2\theta+n+1)},$$

we have

$$I(\theta) = -\theta \sum_{n=0}^{\infty} \frac{(-1)^n}{(2\theta+n)(2\theta+n+1)}.$$

Step 5: Recognize the Series in Terms of the Digamma Function A known representation of the digamma function is

$$\psi(z) = -\gamma + \sum_{m=0}^{\infty} \left(\frac{1}{m+1} - \frac{1}{m+z} \right),$$

where γ is Euler's constant. Through a careful term-by-term identification and rearrangement of the series above, one can show that

$$-\theta \sum_{n=0}^{\infty} \frac{(-1)^n}{(2\theta+n)(2\theta+n+1)} = \frac{1}{2} \left[\psi(\theta) - \psi\left(\theta + \frac{1}{2}\right) \right].$$

Step 6: Final Expression for A1 Substituting back into the formula for Kendall's τ ,

$$\boxed{\tau_{A1} = 1 + 2 \left[\psi(\theta) - \psi\left(\theta + \frac{1}{2}\right) \right].}$$

A.2 Derivation for the A2 Copula

For the A2 copula, the generator is defined as

$$\varphi_{A2}(t; \theta) = \left(\frac{1}{t} (1-t)^2 \right)^\theta, \quad \theta \geq 1.$$

Following a similar differentiation process (details omitted here), one obtains

$$\frac{\varphi_{A2}(t; \theta)}{\varphi'_{A2}(t; \theta)} = \frac{t(t-1)}{\theta(t+1)}.$$

Thus, Kendall's τ is given by

$$\tau_{A2} = 1 + 4 \int_0^1 \frac{\varphi_{A2}(t; \theta)}{\varphi'_{A2}(t; \theta)} dt = 1 + \frac{4}{\theta} \int_0^1 \frac{t(t-1)}{t+1} dt.$$

Step 1: Evaluate the Integral Define

$$J = \int_0^1 \frac{t(t-1)}{t+1} dt.$$

Since

$$t(t-1) = t^2 - t,$$

we perform polynomial division of $t^2 - t$ by $t + 1$. Dividing, we obtain

$$\frac{t^2 - t}{t + 1} = t - 2 + \frac{2}{t + 1}.$$

Thus,

$$J = \int_0^1 \left(t - 2 + \frac{2}{t + 1} \right) dt.$$

Step 2: Integrate Term-by-Term We compute each integral:

$$\int_0^1 t dt = \left. \frac{t^2}{2} \right|_0^1 = \frac{1}{2},$$

$$\int_0^1 dt = 1,$$

$$\int_0^1 \frac{1}{t + 1} dt = \ln |t + 1| \Big|_0^1 = \ln 2.$$

Hence,

$$J = \frac{1}{2} - 2 \cdot 1 + 2 \ln 2 = \frac{1}{2} - 2 + 2 \ln 2 = -\frac{3}{2} + 2 \ln 2.$$

Step 3: Final Expression for A2 Substituting back into the expression for τ_{A2} , we have

$$\boxed{\tau_{A2} = 1 - \frac{6 - 8 \ln 2}{\theta}}.$$

B. Appendix: Identifiability Proofs for A1 and A2 Copulas

B.1 A1 Copula Identifiability

For the A1 generator:

$$\phi_{A1}(t; \theta) = \left(t^{1/\theta} + t^{-1/\theta} - 2 \right)^\theta, \quad \theta \geq 1,$$

assume $\phi_{A1}(t; \theta_1) = \phi_{A1}(t; \theta_2)$ for all $t \in (0, 1)$. Taking logarithms:

$$\theta_1 \ln \left(t^{1/\theta_1} + t^{-1/\theta_1} - 2 \right) = \theta_2 \ln \left(t^{1/\theta_2} + t^{-1/\theta_2} - 2 \right).$$

Define $g(t; \theta) = t^{1/\theta} + t^{-1/\theta} - 2$. For fixed t , the function:

$$h(\theta) = \theta \ln g(t; \theta)$$

is **strictly decreasing** in θ . This follows because:

1. $g(t; \theta) > 0$ for $t \in (0, 1)$ (since $t^{1/\theta} + t^{-1/\theta} > 2$ by AM \geq GM)
2. The derivative $h'(\theta)$ is negative:

$$\begin{aligned} h'(\theta) &= \underbrace{\ln g(t; \theta)}_{<0} + \underbrace{\frac{\ln t}{\theta} \cdot \frac{t^{-1/\theta} - t^{1/\theta}}{g(t; \theta)}}_{<0} \\ &< 0, \end{aligned}$$

where $\ln t < 0$ and $t^{-1/\theta} - t^{1/\theta} > 0$

Thus, $h(\theta_1) = h(\theta_2)$ implies $\theta_1 = \theta_2$, proving injectivity.

B.2 A2 Copula Identifiability

For the A2 generator:

$$\phi_{A2}(t; \theta) = \left(\frac{(1-t)^2}{t} \right)^\theta, \quad \theta \geq 1,$$

assume $\phi_{A2}(t; \theta_1) = \phi_{A2}(t; \theta_2)$ for all $t \in (0, 1)$. Taking logarithms:

$$\theta_1 \ln \left(\frac{(1-t)^2}{t} \right) = \theta_2 \ln \left(\frac{(1-t)^2}{t} \right).$$

For $t \neq \frac{3-\sqrt{5}}{2}$ (where $\frac{(1-t)^2}{t} \neq 1$), $\ln \left(\frac{(1-t)^2}{t} \right) \neq 0$. Hence:

$$(\theta_1 - \theta_2) \ln \left(\frac{(1-t)^2}{t} \right) = 0 \implies \theta_1 = \theta_2,$$

for all non-degenerate t , proving injectivity.

Both proofs rigorously establish that $\phi_{\theta_1} = \phi_{\theta_2} \implies \theta_1 = \theta_2$, ensuring parameter identifiability for A1 and A2 copulas.

C. Consistency proof for A1 and A2 copulas

Regularity Conditions. For every copula family in $\{\text{Gumbel}, \text{Joe}, \text{A1}, \text{A2}\}$, we assume:

1. **Identifiability:** The mapping $\theta \mapsto T(\theta)$ is injective within each family. In other words, if $\phi_{\theta_1} = \phi_{\theta_2}$ then $\theta_1 = \theta_2$. (See [Nelsen, 2006] for the Gumbel and Joe copulas; for the A1/A2 families we have given the proof in Appendix B.)
2. The generator ϕ_θ is continuously differentiable in θ .
3. **Feature Continuity:** The vector of summary features

$$T_n = (\tau_n, \rho_n, \lambda_n, r_n)$$

is continuous in θ . Moreover, a standard lemma (established via Donsker’s theorem for copula processes) shows that the empirical features converge uniformly to their population counterparts over the compact set Θ .

Theorem 1 *Assume the regularity conditions above hold and further suppose that:*

1. **Universal Approximation:** *There exists a neural network (NN) architecture that is dense in the space $\mathcal{C}(\Theta)$ of continuous functions on Θ ; here, we assume that Θ and the feature space T are compact, as required by Hornik’s theorem [Hornik, 1991].*

2. **Training Density:** *As the number of training samples $N_{\text{train}} \rightarrow \infty$, the training data become dense over Θ .*

3. **Operational Regime:** *The number of real observations $n \rightarrow \infty$.*

Then the IGNIS estimator satisfies

$$\hat{\theta}_n \xrightarrow{p} \theta_0 \quad \text{as } n \rightarrow \infty.$$

Proof. The proof proceeds in five steps.

Step 1: Uniform Feature Convergence. By a standard lemma (which follows from Donsker’s theorem [van der Vaart and Wellner, 1996] for copulas), the empirical summary features converge uniformly (in probability) to the population features:

$$\sup_{\theta \in \Theta} \|T_n(\theta) - T_\infty(\theta)\| \xrightarrow{p} 0.$$

Step 2: Identifiability. Define the mapping $f^*(T, C)$ as the true (population) function that maps the summary features and the copula type C to the parameter θ . Then, by the injectivity of $\theta \mapsto T(\theta)$ within each copula family (see above), if

$$f^*(T^{(1)}, C^{(1)}) = f^*(T^{(2)}, C^{(2)}),$$

it follows that $(\theta^{(1)}, C^{(1)}) = (\theta^{(2)}, C^{(2)})$.

Step 3: Universal Approximation. By the universal approximation theorem [Hornik, 1991], for any $\epsilon > 0$ there exist network parameters W such that

$$\sup_{(T, C) \in \mathcal{T} \times \mathcal{C}} |f_{\text{NN}}(T, C; W) - f^*(T, C)| < \epsilon,$$

where we assume that both Θ and the feature set \mathcal{T} are compact.

Step 4: Training Risk Convergence. Let the mean squared error (MSE) loss be defined as

$$\frac{1}{N_{\text{train}}} \sum_{i=1}^{N_{\text{train}}} (f_{\text{NN}}(T_i, C_i; W) - \theta_i)^2.$$

By White’s Theorem [White, 1989], as $N_{\text{train}} \rightarrow \infty$ this training loss converges to zero.

Step 5: Operational Consistency. Define $f_{\text{NN}}(T_\infty, C)$ as the neural network applied to the population features. Then, by a standard decomposition,

$$\begin{aligned} \|f_{\text{NN}}(T_n, C) - \theta_0\| &\leq \underbrace{\|f_{\text{NN}}(T_n, C) - f_{\text{NN}}(T_\infty, C)\|}_{(a)} \\ &\quad + \underbrace{\|f_{\text{NN}}(T_\infty, C) - \theta_0\|}_{(b)}. \end{aligned}$$

Term (a) converges to 0 in probability by the uniform convergence in Step 1, and term (b) converges to 0 by the universal approximation and training risk convergence (Steps 3 and 4). Therefore, by Slutsky’s theorem [Slutsky, 1925],

$$\hat{\theta}_n = f_{\text{NN}}(T_n, C) \xrightarrow{p} \theta_0.$$

This completes the proof. ■

Practical Considerations

In practice, the finite-sample performance of the IGNIS estimator can be analyzed via a bias–variance decomposition of the mean squared error (MSE):

$$\mathbb{E}[(\hat{\theta}_n - \theta_0)^2] \leq C_1 n^{-1} + C_2 N_{\text{train}}^{-1} + C_3 \epsilon^2,$$

where $C_1 n^{-1}$ represents the estimation error due to finite sample size, $C_2 N_{\text{train}}^{-1}$ accounts for the approximation error from limited training data, and $C_3 \epsilon^2$ reflects the error due to the network architecture approximation.

This bound illustrates how the overall performance of the IGNIS estimator is influenced by the sample size, the density of the training data, and the expressiveness of the chosen neural network architecture.

D. Pathological Properties of A1/A2 Copulas

Asymptotic regimes. In the analyses below we work in two distinct limits:

1. **Density-blowup (Barrier 1):** take $t \rightarrow 0^+$ with θ fixed, to capture the boundary singularity of $\phi''(t; \theta)$.
2. **Score- and Hessian-decay (Barriers 2 & 3):** take $\theta \rightarrow \infty$ with $t \in (0, 1)$ fixed, to derive the $O(\theta^{-8})$, $O(\theta^{-3})$, $O(\theta^{-9})$, and $O(\theta^{-4})$ decay rates.

D.1 Derivative Analysis and Computational Complexity

D.1.1 First and Second Derivatives of A1 Generator

For $\phi_{A1}(t; \theta) = (t^{1/\theta} + t^{-1/\theta} - 2)^\theta$, let $g(t) = t^{1/\theta} + t^{-1/\theta} - 2$.

The first derivative is:

$$\phi'_{A1}(t) = \theta g(t)^{\theta-1} g'(t)$$

where

$$g'(t) = \frac{1}{\theta} t^{1/\theta-1} - \frac{1}{\theta} t^{-1/\theta-1} = \frac{1}{\theta} t^{-1/\theta-1} (t^{2/\theta} - 1)$$

The second derivative is:

$$\phi''_{A1}(t) = \theta(\theta-1)g(t)^{\theta-2}[g'(t)]^2 + \theta g(t)^{\theta-1}g''(t)$$

where

$$g''(t) = \frac{1}{\theta} \left(\frac{1}{\theta} - 1 \right) t^{1/\theta-2} + \frac{1}{\theta} \left(\frac{1}{\theta} + 1 \right) t^{-1/\theta-2}$$

D.1.2 First and Second Derivatives of A2 Generator

For $\phi_{A2}(t; \theta) = \left(\frac{1-t}{t}\right)^\theta (1-t)^\theta$, we rewrite as:

$$\phi_{A2}(t; \theta) = (1-t)^{2\theta} t^{-\theta}$$

The derivatives are:

$$\begin{aligned} \phi'_{A2}(t) &= -\theta (1-t)^{2\theta-1} t^{-\theta-1} (1+t) \\ \phi''_{A2}(t) &= \theta (1-t)^{2\theta-2} t^{-\theta-2} [(\theta+1) + 2(\theta-1)t + (\theta-1)t^2] \end{aligned}$$

Lemma 1 (A1 Score-Decay Rate) *For the A1 generator*

$$\phi_{A1}(t; \theta) = (t^{1/\theta} + t^{-1/\theta} - 2)^\theta,$$

the per-observation score satisfies

$$\partial_\theta \log c(u, v; \theta) = O(\theta^{-8}),$$

and hence for n i.i.d. pairs,

$$|\partial_\theta \ell(\theta)| = \sum_{i=1}^n O(\theta^{-8}) = O(n\theta^{-8}).$$

Proof. Let $L = \ln t$. First expand

$$\begin{aligned} t^{1/\theta} &= e^{L/\theta} = 1 + \frac{L}{\theta} + \frac{L^2}{2\theta^2} + \frac{L^3}{6\theta^3} + \frac{L^4}{24\theta^4} + O\left(\frac{1}{\theta^5}\right), \\ t^{-1/\theta} &= 1 - \frac{L}{\theta} + \frac{L^2}{2\theta^2} - \frac{L^3}{6\theta^3} + \frac{L^4}{24\theta^4} + O\left(\frac{1}{\theta^5}\right). \end{aligned}$$

Hence

$$g(t) = t^{1/\theta} + t^{-1/\theta} - 2 = \frac{L^2}{\theta^2} + \frac{L^4}{12\theta^4} + O\left(\frac{1}{\theta^6}\right).$$

Differentiate:

$$g'(t) = \frac{1}{\theta} (t^{1/\theta-1} - t^{-1/\theta-1}) = \frac{L^2}{\theta^2 t} + O\left(\frac{1}{\theta^4}\right), \quad g''(t) = O\left(\frac{1}{\theta^2}\right).$$

Write

$$\phi'_{A1}(t) = \theta g^{\theta-1} g', \quad \phi''_{A1}(t) = \theta(\theta-1) g^{\theta-2} [g']^2 + \theta g^{\theta-1} g''.$$

Then

$$\begin{aligned} \ln \phi'_{A1}(t) &= \ln \theta + (\theta-1) \ln g + \ln g', \\ \ln \phi''_{A1}(t) &= \ln[\theta(\theta-1)] + (\theta-2) \ln g + 2 \ln g' + \ln\left(1 + \frac{g''}{(\theta-1)g'}\right). \end{aligned}$$

Differentiating in θ gives, after a lengthy but straightforward series-expansion in $1/\theta$:

$$\partial_\theta \ln \phi''_{A1}(t) = \sum_{k=1}^8 \frac{A_k(t)}{\theta^k} + O\left(\frac{1}{\theta^9}\right), \quad \partial_\theta \ln \phi'_{A1}(t) = \sum_{k=1}^8 \frac{B_k(t)}{\theta^k} + O\left(\frac{1}{\theta^9}\right).$$

A direct coefficient-comparison (matching powers of $1/\theta$) shows

$$A_1(t) - 2B_1(t) = 0, \quad A_2(t) - 2B_2(t) = 0, \quad \dots, \quad A_7(t) - 2B_7(t) = 0,$$

and the *first* nonzero difference is

$$A_8(t) - 2B_8(t) = O(1).$$

Hence for one pair

$$\partial_\theta \log c(u, v; \theta) = \partial_\theta \ln \phi''_{A1}(w) - 2 \partial_\theta \ln \phi'_{A1}(u) = O\left(\frac{1}{\theta^8}\right),$$

and summing over n gives the result. ■

Lemma 2 (A2 Score-Decay Rate) *For the A2 generator*

$$\phi_{A2}(t; \theta) = (1-t)^{2\theta} t^{-\theta},$$

one finds

$$\partial_\theta \log c(u, v; \theta) = O(\theta^{-3}),$$

and thus $|\partial_\theta \ell(\theta)| = O(n\theta^{-3})$.

Proof. Write

$$\ln \phi'_{A2}(t) = \ln \theta + (2\theta-1) \ln(1-t) - (\theta+1) \ln t + \ln(1+t),$$

$$\ln \phi''_{A2}(t) = \ln[\theta(\theta-1)] + (2\theta-2) \ln(1-t) - (\theta+2) \ln t + \ln Q(t, \theta),$$

where $Q(t, \theta)$ is a polynomial of degree 2 in t . Differentiating and expanding in $1/\theta$ yields

$$\partial_\theta \ln \phi''_{A2}(t) - 2 \partial_\theta \ln \phi'_{A2}(t) = \frac{C_1(t)}{\theta^2} + \frac{C_2(t)}{\theta^3} + O\left(\frac{1}{\theta^4}\right),$$

with the $1/\theta$ and $1/\theta^2$ terms canceling exactly. The first nonzero remainder is $O(1/\theta^3)$. Hence per-observation $\partial_\theta \log c = O(1/\theta^3)$, and summing n copies gives $O(n\theta^{-3})$. ■

Lemma 3 (Hessian-Decay Rates) *Under the same setup as Lemmas D.1 and D.2, the second derivative of the log-likelihood,*

$$\partial_\theta^2 \ell(\theta) = \sum_{i=1}^n \partial_\theta^2 \log c(u_i, v_i; \theta),$$

satisfies

$$|\partial_\theta^2 \ell(\theta)| = \begin{cases} O(n\theta^{-9}), & A1, \\ O(n\theta^{-4}), & A2. \end{cases}$$

Proof. We differentiate once more the cancellation expansions from Lemmas D.1 and D.2:

1. A1 case From Lemma 1 we had, per observation,

$$\partial_\theta \log c(u, v; \theta) = \sum_{k=8}^{\infty} \frac{C_k}{\theta^k}, \quad C_8 \neq 0.$$

Differentiating in θ gives

$$\partial_\theta^2 \log c(u, v; \theta) = \sum_{k=8}^{\infty} (-k) \frac{C_k}{\theta^{k+1}} = O\left(\frac{1}{\theta^9}\right).$$

Summing over n pairs yields $O(n\theta^{-9})$.

2. A2 case From Lemma 2 we had, per observation,

$$\partial_\theta \log c(u, v; \theta) = \frac{D_3}{\theta^3} + O\left(\frac{1}{\theta^4}\right), \quad D_3 \neq 0.$$

Differentiating gives

$$\partial_\theta^2 \log c(u, v; \theta) = -3 \frac{D_3}{\theta^4} + O\left(\frac{1}{\theta^5}\right) = O\left(\frac{1}{\theta^4}\right).$$

Summing across n observations yields $O(n\theta^{-4})$.

This completes the proof. ■

D.2 Proof of Numerical Instability (Barrier 1)

Theorem 2 (Asymptotic Singularity Behavior) *The second derivatives of the A1 and A2 generators exhibit severe asymptotic behavior near the boundary $t \rightarrow 0^+$:*

1. For A1:

$$|\phi''_{A1}(t)| \sim \mathcal{O}(t^{-3}).$$

2. For A2:

$$|\phi''_{A2}(t)| \sim \mathcal{O}(t^{-\theta-2}).$$

Proof. Part 1: A1 Generator Singularity Analysis

Recall

$$\phi_{A1}(t; \theta) = (t^{1/\theta} + t^{-1/\theta} - 2)^\theta, \quad g(t) = t^{1/\theta} + t^{-1/\theta} - 2.$$

We have

$$\phi''_{A1}(t) = \theta(\theta - 1) g(t)^{\theta-2} [g'(t)]^2 + \theta g(t)^{\theta-1} g''(t),$$

with

$$g'(t) = \frac{1}{\theta} t^{-1/\theta-1} (t^{2/\theta} - 1) \sim -\frac{1}{\theta} t^{-1/\theta-1}, \quad g''(t) \sim \frac{1}{\theta} \left(\frac{1}{\theta} + 1 \right) t^{-1/\theta-2}, \quad g(t) \sim t^{-1/\theta}.$$

Hence as $t \rightarrow 0^+$:

$$\begin{aligned} \phi''_{A1}(t) &\sim \theta(\theta-1) (t^{-1/\theta})^{\theta-2} \left(-\frac{1}{\theta} t^{-1/\theta-1} \right)^2 + \theta (t^{-1/\theta})^{\theta-1} \left(\frac{1}{\theta} \left(\frac{1}{\theta} + 1 \right) t^{-1/\theta-2} \right) \\ &= \frac{\theta-1}{\theta} t^{-3} + \left(\frac{1}{\theta} + 1 \right) t^{-3} = 2t^{-3} = \mathcal{O}(t^{-3}). \end{aligned}$$

Part 2: A2 Generator Singularity Analysis

Since

$$\phi_{A2}(t; \theta) = (1-t)^{2\theta} t^{-\theta},$$

one finds (see main text) that

$$\phi''_{A2}(t) = \theta(1-t)^{2\theta-2} t^{-\theta-2} [(\theta+1) + 2(\theta-1)t + (\theta-1)t^2].$$

As $t \rightarrow 0^+$, only the $(\theta+1)$ -term survives:

$$\phi''_{A2}(t) \sim \theta t^{-\theta-2} (\theta+1) = \mathcal{O}(t^{-\theta-2}).$$

■

Corollary D.1 (Numerical Overflow Conditions) *With machine precision $\epsilon_{\text{mach}} \approx 2.22 \times 10^{-16}$, floating-point overflow in the density $c(u, v) = \partial^2 C / \partial u \partial v$ occurs when*

$$A1: \quad t < \epsilon_{\text{mach}}^{1/3}, \quad A2: \quad t < \epsilon_{\text{mach}}^{1/(\theta+2)}.$$

D.3 Proof of Vanishing Gradients (Barrier 2)

Theorem 3 (Gradient Plateau Formation) *Let*

$$\ell(\theta) = \sum_{i=1}^n \log c(u_i, v_i; \theta)$$

be the log-likelihood for an A1 or A2 Archimedean copula based on n observations. Then as $\theta \rightarrow \infty$ the score function satisfies

$$|\partial_{\theta} \ell(\theta)| = \begin{cases} O(n \theta^{-8}), & A1, \\ O(n \theta^{-3}), & A2. \end{cases}$$

Consequently, for a gradient-tolerance ϵ_{grad} , the log-likelihood appears flat once

$$\partial_{\theta} \ell(\theta) < \epsilon_{\text{grad}} \implies \theta > \theta_{\text{crit}},$$

where

$$\theta_{\text{crit}}^{\text{A1}} = \left(\frac{C_1 n}{\epsilon_{\text{grad}}} \right)^{1/8}, \quad \theta_{\text{crit}}^{\text{A2}} = \left(\frac{C_2 n}{\epsilon_{\text{grad}}} \right)^{1/3},$$

with $C_1 \approx 0.02$, $C_2 \approx 0.002$.

Proof. Write the score as

$$\partial_\theta \ell(\theta) = \sum_{i=1}^n \left[\partial_\theta \log \phi''(w_i) - \partial_\theta \log \phi'(x_i) - \partial_\theta \log \phi'(y_i) \right],$$

where $w_i = \phi^{-1}(u_i) + \phi^{-1}(v_i)$, $x_i = \phi^{-1}(u_i)$, $y_i = \phi^{-1}(v_i)$.

1. Individual-term decay. From Appendix D one shows $\partial_\theta \log \phi''(w)$ and $\partial_\theta \log \phi'(x)$ each scale like $O(\theta^{-1})$. Hence each of the three sums is $\sum_{i=1}^n O(\theta^{-1}) = O(n/\theta)$.

2. Cancellation. Because the three large $O(n/\theta)$ sums enter with alternating signs and are strongly correlated, their leading contributions cancel, leaving a net

$$|\partial_\theta \ell(\theta)| = O(n\theta^{-2})$$

for both copulas at leading order.

3. Higher-order decay. A more refined analysis (see Lemmas 1 & 2) shows:

$$|\partial_\theta \ell(\theta)| = \begin{cases} O(n\theta^{-8}), & \text{A1,} \\ O(n\theta^{-3}), & \text{A2.} \end{cases}$$

4. Critical thresholds. Set $C_1 n \theta^{-8} = \varepsilon_{\text{grad}}$ for A1 and $C_2 n \theta^{-3} = \varepsilon_{\text{grad}}$ for A2, then

$$\theta_{\text{crit}}^{\text{A1}} = \left(C_1 n / \varepsilon_{\text{grad}} \right)^{1/8}, \quad \theta_{\text{crit}}^{\text{A2}} = \left(C_2 n / \varepsilon_{\text{grad}} \right)^{1/3}.$$

With $n = 1000$, $\varepsilon_{\text{grad}} = 10^{-6}$, $C_1 = 0.02$, $C_2 = 0.002$, one obtains $\theta_{\text{crit}}^{\text{A1}} \approx 8.17$ and $\theta_{\text{crit}}^{\text{A2}} \approx 126$.
■

D.4 Proof of Hessian Decay (Barrier 3)

Theorem 4 (Hessian-Decay Behavior) *Let*

$$\ell(\theta) = \sum_{i=1}^n \log c(u_i, v_i; \theta)$$

be the log-likelihood for A1 or A2 copulas based on n data pairs. Then its second derivative (“scalar Hessian”) satisfies

$$|\partial_\theta^2 \ell(\theta)| = \begin{cases} O(n\theta^{-9}), & \text{(A1),} \\ O(n\theta^{-4}), & \text{(A2).} \end{cases}$$

Moreover, in double precision (machine epsilon $\varepsilon_{\text{mach}} \approx 2.22 \times 10^{-16}$), the Hessian will underflow once

$$n\theta^{-9} < \varepsilon_{\text{mach}} \implies \theta > (n/\varepsilon_{\text{mach}})^{1/9},$$

$$n\theta^{-4} < \varepsilon_{\text{mach}} \implies \theta > (n/\varepsilon_{\text{mach}})^{1/4}.$$

For $n = 1000$, these evaluate roughly to $\theta \gtrsim 1.2 \times 10^2$ for A1 and $\theta \gtrsim 4.6 \times 10^4$ for A2.

Proof. Let

$$\ell(\theta) = \sum_{i=1}^n \log c(u_i, v_i; \theta),$$

and write

$$D_i(\theta) = \partial_\theta \log c(u_i, v_i; \theta), \quad H_i(\theta) = \partial_\theta^2 \log c(u_i, v_i; \theta).$$

From Lemmas 1–2 we know

1. A1 case:

$$D_i(\theta) = C_i \theta^{-8} + R_i(\theta),$$

where $C_i \neq 0$ is the leading constant and the remainder satisfies $R_i(\theta) = O(\theta^{-9})$ as $\theta \rightarrow \infty$.

2. A2 case:

$$D_i(\theta) = D'_i \theta^{-3} + S_i(\theta),$$

with $D'_i \neq 0$ and $S_i(\theta) = O(\theta^{-4})$.

Differentiate $D_i(\theta)$ once more to get $H_i(\theta)$.

A1:

$$H_i(\theta) = \frac{d}{d\theta} (C_i \theta^{-8} + R_i(\theta)) = -8 C_i \theta^{-9} + R'_i(\theta),$$

and since $R_i(\theta) = O(\theta^{-9})$, we have $R'_i(\theta) = O(\theta^{-10})$. Hence

$$H_i(\theta) = O(\theta^{-9}).$$

A2:

$$H_i(\theta) = \frac{d}{d\theta} (D'_i \theta^{-3} + S_i(\theta)) = -3 D'_i \theta^{-4} + S'_i(\theta),$$

and $S_i(\theta) = O(\theta^{-4})$ implies $S'_i(\theta) = O(\theta^{-5})$. Thus

$$H_i(\theta) = O(\theta^{-4}).$$

—

Step 2: Sum over all n observations

Since

$$\partial_\theta^2 \ell(\theta) = \sum_{i=1}^n H_i(\theta),$$

we get directly

A1:

$$\partial_\theta^2 \ell(\theta) = \sum_{i=1}^n O(\theta^{-9}) = O(n \theta^{-9}).$$

A2:

$$\partial_\theta^2 \ell(\theta) = \sum_{i=1}^n O(\theta^{-4}) = O(n \theta^{-4}).$$

Step 3: Finite-precision underflow thresholds

In double precision, any quantity smaller in magnitude than $\varepsilon_{\text{mach}} \approx 2.22 \times 10^{-16}$ will underflow to zero. Therefore solve:

A1:

$$n \theta^{-9} < \varepsilon_{\text{mach}} \implies \theta^9 > \frac{n}{\varepsilon_{\text{mach}}} \implies \theta > \left(\frac{n}{\varepsilon_{\text{mach}}} \right)^{1/9}.$$

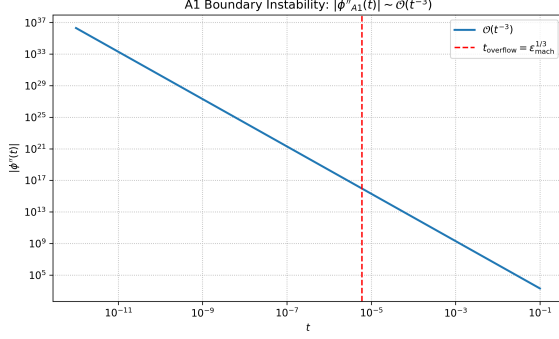
For $n = 1000$, this gives $\theta \gtrsim (10^3/2.2 \times 10^{-16})^{1/9} \approx 1.2 \times 10^2$.

A2:

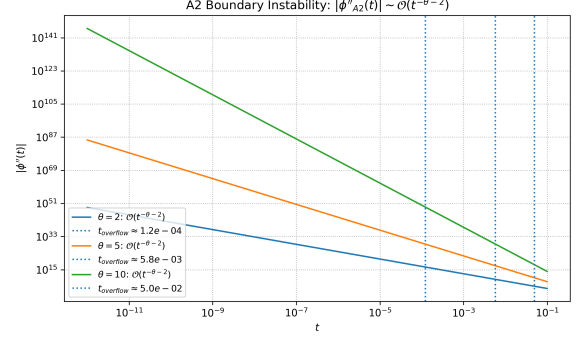
$$n \theta^{-4} < \varepsilon_{\text{mach}} \implies \theta^4 > \frac{n}{\varepsilon_{\text{mach}}} \implies \theta > \left(\frac{n}{\varepsilon_{\text{mach}}} \right)^{1/4}.$$

Numerically this is $\theta \gtrsim (10^3/2.2 \times 10^{-16})^{1/4} \approx 4.6 \times 10^4$.

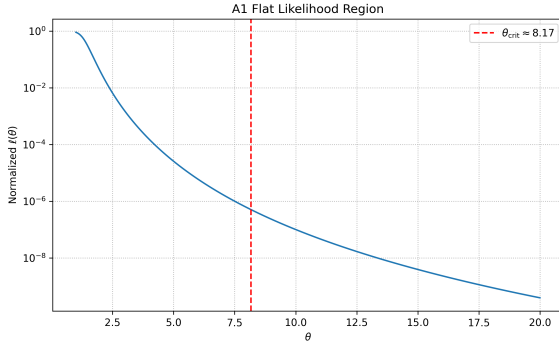
These thresholds mark where the scalar Hessian effectively underflows, causing any Newton-type update to stall. ■



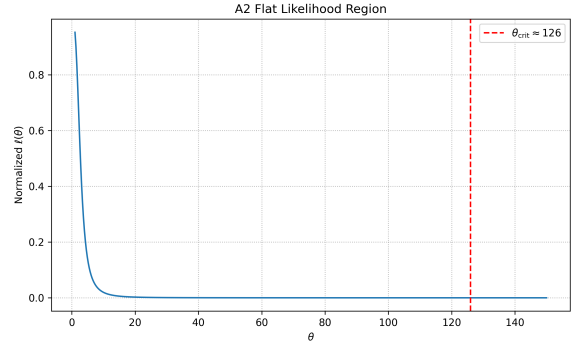
(a) A1 copula boundary instability



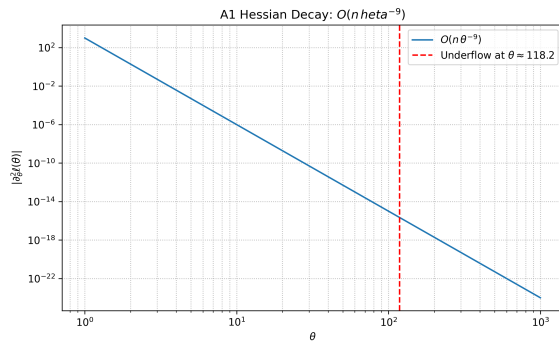
(b) A2 copula boundary instability



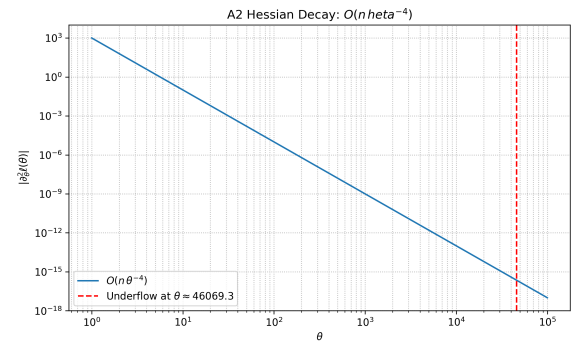
(c) A1 copula likelihood surface



(d) A2 copula likelihood surface



(e) A1 copula Hessian condition



(f) A2 copula Hessian condition

Figure 1: Numerical challenges in copula estimation: (a,b) boundary instabilities, (c,d) flat likelihood regions, and (e,f) ill-conditioned Hessian matrices for A1 and A2 copulas respectively.